Available online at www.sciencedirect.com
ScienceDirect
Trans. Nonferrous Met. Soc. China 32(2022) 2578−2586
Transactions of Nonferrous Metals Society of China
www.tnmsc.cn

Effect of electropulsing on anisotropy in strength of laser metal deposited Ti−6Al−4V alloy

Fu-bin WANG[1], Yu-ke LIU[1], Yun-xiang TONG[1], Chong ZHANG[1], Feng-chun JIANG[2], Jian-dong WANG[2]

1. Institute of Materials Processing and Intelligent Manufacturing, College of Materials Science and Chemical Engineering, Harbin Engineering University, Harbin 150001, China;
2. Key Laboratory of Superlight Materials and Surface Technology, Ministry of Education, College of Material Science and Chemical Engineering, Harbin Engineering University, Harbin 150001, China

Received 3 August 2021; accepted 7 December 2021

Abstract: The effect of electropulsing treatment on microstructure and mechanical strength of laser metal deposited Ti−6Al−4V alloy was investigated in order to eliminate the anisotropy in strength of laser metal deposited Ti−6Al−4V alloy by tensile tests, optical microscopy, scanning electron microscopy, electron back-scattered diffraction analyses and transmission electron microscopy. With increasing applied voltages from 0 to 130 V, the evolution of microstructure within columnar β grains followed the sequence of α' martensite → colony α structure → basket-weave α structure. The electropulsing treated at 130 V weakened the texture of martensite within β grains. The as-built Ti−6Al−4V alloy showed an anisotropy in yield strength (6.2%). After processing at 130 V, the anisotropy in yield strength was reduced to 0.6%, which was attributed to the almost equivalent distribution of Schmid factor in the samples deformed along different orientations.

Key words: laser metal deposition; Ti−6Al−4V alloy; yield strength; anisotropy; electropulsing

1 Introduction

Additively manufactured (AM) Ti−6Al−4V alloys have attracted much attentions in engineering and biomedical fields due to their advantages in design and manufacturing of components with complex geometry and minimal material waste etc [1−5]. Among various additive manufacturing techniques, laser metal deposition (LMD) has a high degree of control and convenience in compositional design [2,5−7]. The as-built Ti−6Al−4V alloy fabricated via LMD processing is typically characterized by the anisotropic microstructure consisting of coarse and columnar β grains along building direction [8,9], resulting from the intrinsic high cooling rate and high thermal gradient, which usually leads to mechanical property anisotropy, including yield strength (YS) and elongation [10,11]. This undesirable anisotropy obviously hinders the applications of AM Ti−6Al−4V alloys in the conditions requiring mechanical isotropy.

To date, several in-situ or post-processing methods have been proposed to achieve isotropic microstructure in AM Ti−6Al−4V alloys, including introduction of high-density ultrasound [11], using blends of Ti−6Al−4V and Co−Cr−Mo powders [12], and rapid heat treatment [13]. During deposition, introducing high-density ultrasound is beneficial to obtaining a fully equiaxed and refined structure without preferred orientation by activating nuclei,

Corresponding author: Yun-xiang TONG, Tel: +86-451-82518644, E-mail: tongyx@hrbeu.edu.cn;
Jian-dong WANG, Tel: +86-451-82518644, E-mail: wangjiandong@hrbeu.edu.cn
DOI: 10.1016/S1003-6326(22)65967-3

thus enhancing mechanical strength and isotropy simultaneously [11]. In general, reducing the driving force for heterogeneous nucleation during solidification is effective in achieving equiaxed microstructure [14]. Following this rule, AM Ti-based alloys characterized by the equiaxed grains with random orientations and isotropic mechanical properties have been obtained by using blends of Ti−6Al−4V and Co−Cr−Mo powders [12]. Rapid heat treatment above β transus temperature was also used to tailor the microstructure and mechanical behavior of Ti−6Al−4V alloy fabricated by laser powder-bed fusion [13,15]. The results show that texture can be weakened due to epitaxial recrystallization [13].

Electropulsing treatment has been recognized as an effective method to enhance formability of conventionally-deformed metals through defect-level microstructural reconfiguration [16]. Very recently, WARYOBA et al [17] reported that the proper electropulsing can increase grain size and enhance microhardness simutaneously of Ti−6Al−4V alloy fabricated by laser-powder bed fusion, which was attributed to the athermal effects due to high electron wind force. In addition, GAO et al [18] reported that electropulsing causes the change of β grains from columnar structure to equiaxed one for selective laser melted Ti−6Al−4V alloy. The aforementioned results imply that electropulsing can also be used to tailor the microstructure of AM alloys.

As one of the important mechanical properties, YS is of crucial importance for engineering applications. It has been reported that the YS of as-built Ti alloys can be dominated by the texture of α lath, especially the anisotropy in YS [19]. However, to the best of our knowledge, the effect of electropulsing on microstructure and YS of laser metal deposited Ti−6Al−4V alloy has less been investigated yet. In the present work, laser metal deposited Ti−6Al−4V alloy was treated by electropulsing at different applied voltages. The relationship between anisotropy of mechanical properties and crystallographic orientation was established on the basis of the evolution of Schmid factor (SF) of different deformation directions. The present work may provide an alternative and efficient way to optimize the mechanical properties of AM alloys.

2 Experimental

The materials used for this work were Ti−6Al−4V powders with a diameter of 45−100 μm. The as-built samples were fabricated by a self-made LMD system under an argon atmosphere. The following processing parameters, i.e. a laser power of 1200 W, a laser spot size of 4 mm, a scanning velocity of 5.8 mm/s, and a powder feed rate of 4.5 g/min, were used. The as-built thin wall was deposited on Ti−6Al−4V substrate by single layer-by-layer method. After processing, the as-built Ti−6Al−4V thin wall samples were cut into the samples for electropulsing treatment with a length of 90 mm, a width of 4 mm and a height of 15 mm. The voltages of 100 and 130 V were used, and the frequency and duration were fixed at 350 Hz and 20 s, respectively. The current was applied along the laser scanning direction, as schematically shown in Fig. 1(a).

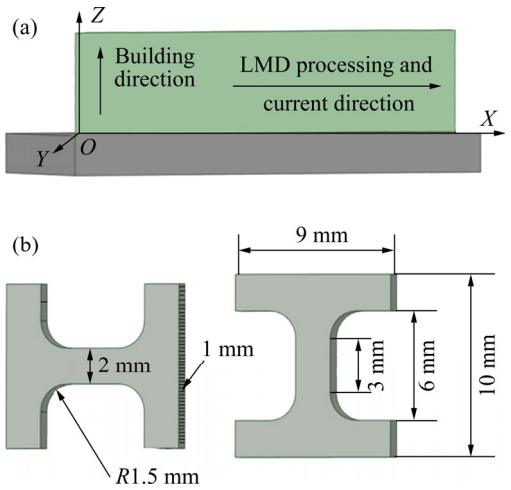

Fig. 1 Schematic illustration of thin wall sample geometry (a) and dog-bone-shaped tensile samples (b)

Mechanical properties were measured by a tensile machine (Zwick Z2.5 TH). The dog-bone-shaped samples with gauge dimensions of 3 mm × 2 mm × 1 mm were cut along *OX* and *OZ* directions, respectively (Fig. 1(b)). A laser extensometer with a gauge length of 2 mm was used to measure the strain during tensile deformation. Three samples for each processing condition were deformed and the average strength was reported. The strain rate was fixed at 0.5×10^{-3} s^{-1}. The observation of microstructure was carried out on the *YOZ* plane using a MDJ 200

optical microscope and a Thermo Fisher scanning electron microscope (SEM). The samples were prepared by mechanical grinding, polishing and etching with a solution consisting of 10% HF, 30% HNO_3 and 60% H_2O in volume fraction. The crystallographic texture of the samples was characterized by electron back-scattered diffraction (EBSD) analyses using a JSM 7100F scanning electron microscope operated at 20 kV. The step size was fixed at 0.25 μm. The samples for EBSD analyses were prepared by electrochemical polishing. Transmission electron microscopy (TEM) observations were conducted on a FEI Talos 200 FX G2 transmission electron microscope operated at 200 kV. TEM foils were prepared by mechanical grinding followed by ion milling.

3 Results and discussion

3.1 Mechanical properties

Table 1 summarizes the YS and ultimate tensile strength (UTS) of the differently processed samples. The strength of the as-built sample is orientation-dependent. When deformed along *OX* direction, the as-built sample showed a YS of (945±20) MPa. When deformed along *OZ* direction, a YS of (886±23) MPa was obtained. The effect of deformation direction on YS agrees well with the reported results for as-built Ti−6Al−4V alloy [9,20]. It is suggested that the orientation-dependence of YS is caused by the texture of α'/α lath. The mechanical strengths of the as-built samples are close to the reported results [9,21]. After processing at 100 V, both the YS and UTS slightly decreased. After processing at 130 V, the YS decreased, irrespective of deformation direction. The above results indicate that electropulsing treatment is effective in tailoring the mechanical strength for laser metal deposited samples. The anisotropy in YS is defined by $(\sigma_{OX}-\sigma_{OZ})/\sigma_{OX}$, in which σ_{OX} and σ_{OZ} are the YS values along *OX* and *OZ* directions, respectively [10]. With increasing applied voltage to 130 V, the anisotropy in YS decreased from 6.2% to 0.6%, as shown in Table 1. These results clearly indicate that electropulsing treatment is powerful in weakening the strength anisotropy of laser metal deposited Ti−6Al−4V alloy.

Table 1 Mechanical strength and anisotropy in YS for different samples

Sample	YS/MPa	UTS/MPa	Anisotropy in YS/%
As-built, *OX*	945±20	1033±29	6.2
As-built, *OZ*	886±23	1001±12	
100 V, *OX*	905±25	1000±39	4.4
100V, *OZ*	865±7	972±19	
130V, *OX*	879±7	1041±9	0.6
130V, *OZ*	874±4	1025±25	

3.2 Microstructure

In order to understand the effect of electropulsing on the mechanical properties of different Ti−6Al−4V samples, microstructure characterization was first carried out. Figure 2 shows the optical microscopy images of different samples. The as-built sample exhibited the columnar prior-β grains along the building direction,

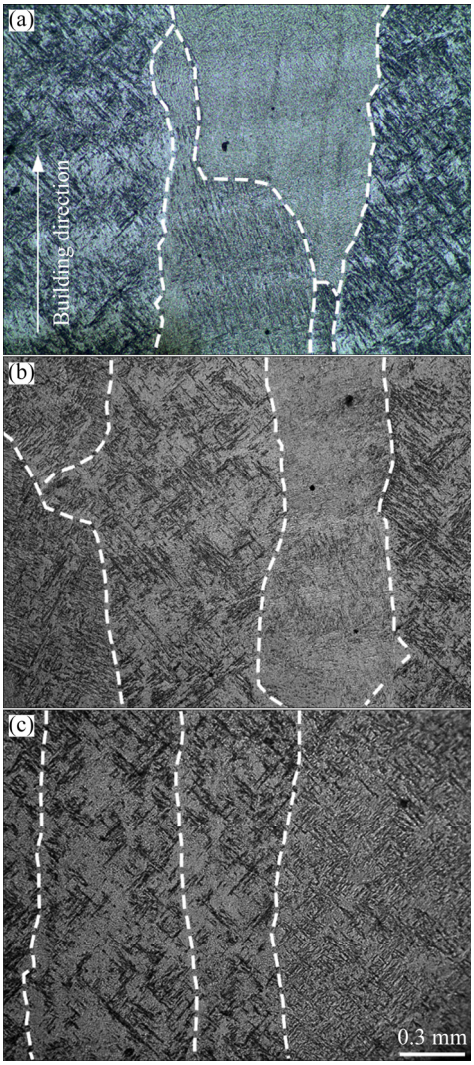

Fig. 2 Optical micrographs of as-built sample (a), and samples processed at 100 V (b) and 130 V (c)

which is the common feature of as-built Ti−6Al−4V alloy and usually attributed to large temperature gradient and narrow solidification range [2,12]. Electropulsing did not change the morphology of prior-β grains, as shown in Figs. 2(b, c). Another feature is that the width of the columnar prior-β grains (0.5−2 mm) is comparable to the gauge size of the present tensile samples, which falls in the reported range for the coarse prior-β grains (0.2−4 mm) [2]. Therefore, the effect of prior-β grain boundary on strength can be ignored. The YS of the studied samples can be mainly controlled by the microstructure within prior-β grains.

Figure 3 shows the morphology of α lath inside of columnar prior-β grain for different samples. The as-built sample was characterized by the typical martensitic microstructure, being consistent with the reported results [22,23]. The widths of α' laths were determined to be (0.88±0.22) μm. After processing at 100 V, the microstructure consisted of the fine colony structure of α laths with the widths of (0.70±0.22) μm. This is because the samples were air-cooled to room temperature after electropulsing treatment. After processing at 130 V, the typical basket-weave α laths with the widths of (0.70±0.12) μm were clearly observed, as shown in Fig. 3(c). With increasing applied voltages, the average aspect ratio of α'/α lath decreased.

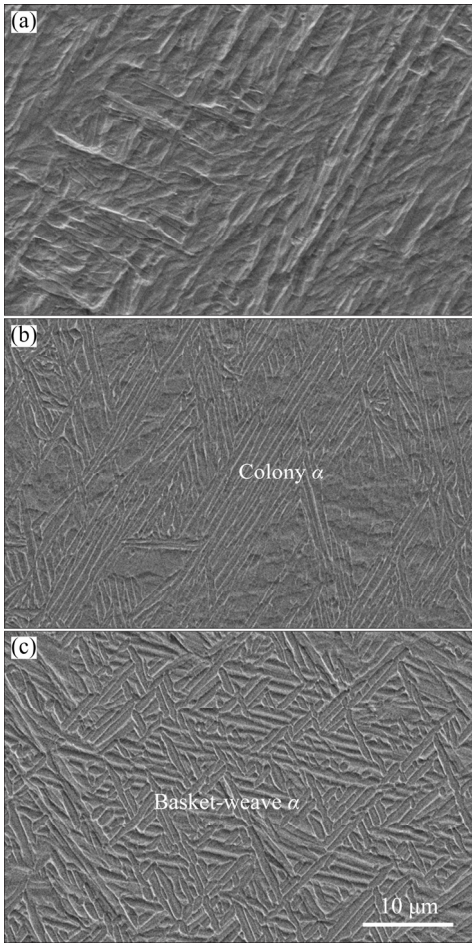

Fig. 3 SEM images of as-built sample (a), and samples processed at 100 V (b) and 130 V (c)

Figure 4 shows the TEM bright field images of different samples and the corresponding selected

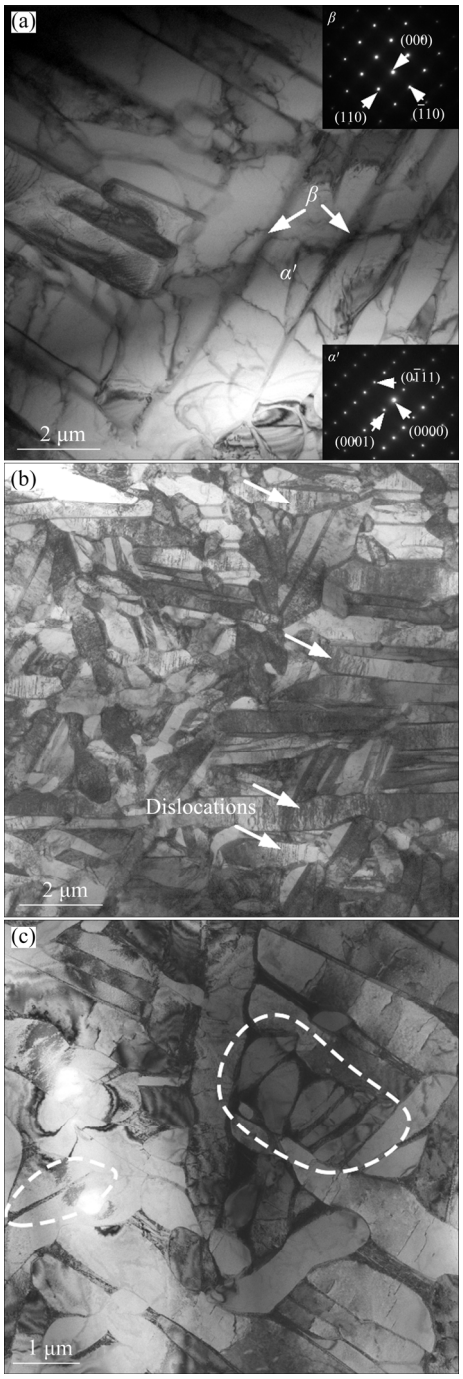

Fig. 4 TEM bright field images of as-built sample (a), and samples processed at 100 V (b) and 130 V (c) (The SAED patterns inserted in (a) indicate the existence of α' lath and β phase)

area electron diffraction (SAED) patterns. The microstructure of the as-built sample is mainly characterized by α' lath and nanoscale β phase located in the channel of lath, which is confirmed by the SAED patterns shown in insets. The α' lath takes a dominant volume fraction, which can be attributed to the high cooling rate of melt pool during LMD processing [2]. After processing at 100 V, a large number of dislocations were observed in the interior of α lath, as indicated by the arrows. Figure 4(c) shows the microstructure of the sample treated at 130 V, which is characterized by the curved interface between α laths, reduced aspect ratio of α lath and dislocation density. The above results clearly show that α'/α lath can be gradually tailored by proper electropulsing treatment. Electropulsing can exert athermal and thermal effects on the samples. The athermal force of electron wind may accelerate the dislocation movement [24]. This is confirmed by the results shown in Fig. 4(b), in which dislocations are generated due to electron wind. With increasing voltage to 130 V, large and localized Joule-heat is produced through obstructing electrons by dislocations, which acts as a thermal grooving to form the low angle boundary [25]. The thermal grooving process may further reduce the amount of α'/α boundary and new α/β interfaces are formed through dislocations arrangement and substructure formation [26]. As a result, β phase diffuses into the groove and splits α lath, as evidenced by the regions circled by dashed lines in Fig. 4(c). Therefore, the slender α laths change to short rods.

Figure 5 shows the inverse pole figures (IPFs) along *OZ* direction of the differently processed samples. From Fig. 5(a), it is seen that $\langle\bar{1}2\bar{1}0\rangle$ fiber texture parallel to the *OZ* direction was formed during LMD. In addition, the texture of $(01\bar{1}2)[01\bar{1}1]$ was identified, being consistent with the previously reported results [27]. The formation of this texture is related to the fact that the direction of grain growth closely aligns with the maximum heat flow during deposition [28]. It is generally accepted that the texture resulting from the energy input during LMD cannot be significantly influenced by conventional heat treatment [29]. However, as shown in Figs. 5(b, c), the grain orientation was changed by the electro-

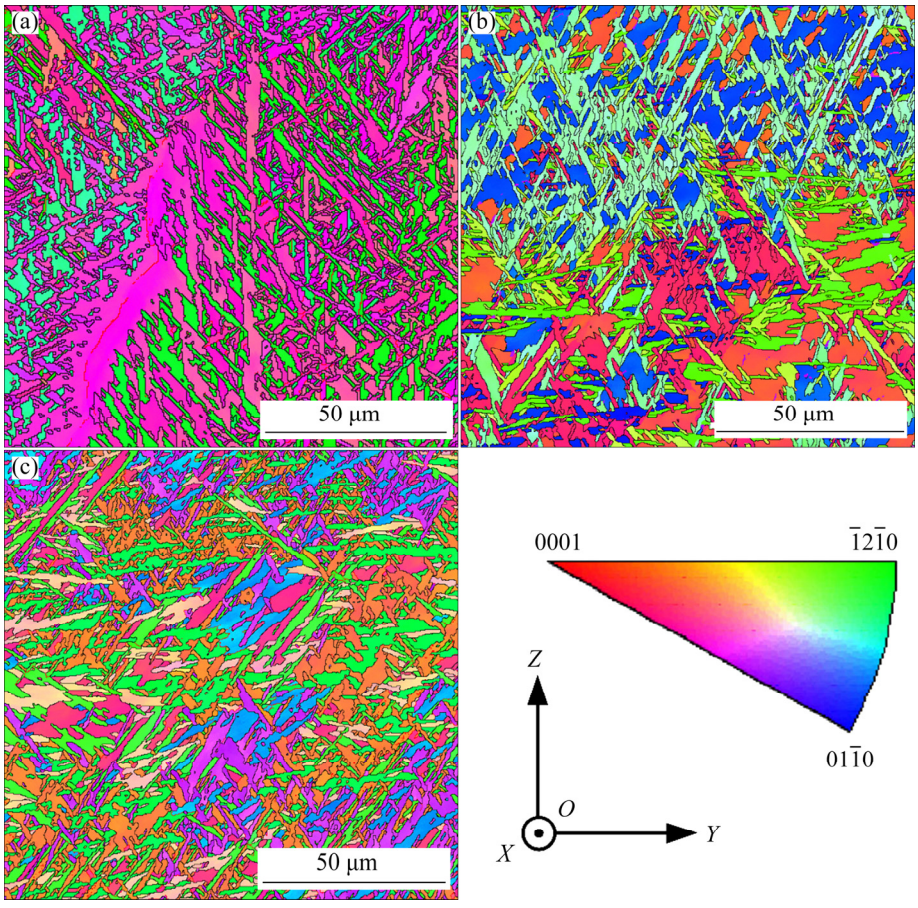

Fig. 5 EBSD IPF maps in *YOZ* plane for as-built sample (a), and samples processed at 100 V (b) and 130 V (c)

pulsing treatment perpendicular to the *YOZ* plane for 20 s. For the sample treated at 100 V, the new $(01\bar{1}0)[12\bar{1}0]$ texture appeared. Meanwhile, the $\langle\bar{1}2\bar{1}0\rangle$ fiber texture resulting from maximum heat flux disappeared. For the sample treated at 130 V, multiple crystallographic orientations appeared in the same direction, indicating that the preferred orientations were weakened.

The evolution of microstructure inevitably influences mechanical properties. In order to understand the dependence of YS on deformation direction for each sample, the Schmid factor (SF) maps for slip system were calculated when the samples were deformed along *OX* and *OZ* directions, as shown in Fig. 6. It has been reported that basal slip is the main deformation mechanism for the anisotropic AM Ti−6Al−4V alloy, and pyramidal slip is for the isotropic one [20]. Therefore, the SF maps for the basal slip were provided for the as-built sample and that processed at 100 V, and the SF maps of pyramidal slip were chosen for that processed at 130 V. In SF maps, red color corresponds to "soft" (easy to activate slip system) orientation, and blue color "hard" (difficult to activate slip system) orientation. It is seen that for the as-built sample and the sample processed at 100 V, the "soft" α lath regions were mixed with the "hard" regions. For the sample processed at 130 V, the "soft" α lath occupied most of regions of Figs. 6(g, h), irrespective of deformation directions.

According to the statistical result of SF shown in Figs. 6(c, f), in the as-built sample and the sample processed at 100 V, the distribution of SF is totally different for the tensile deformations along

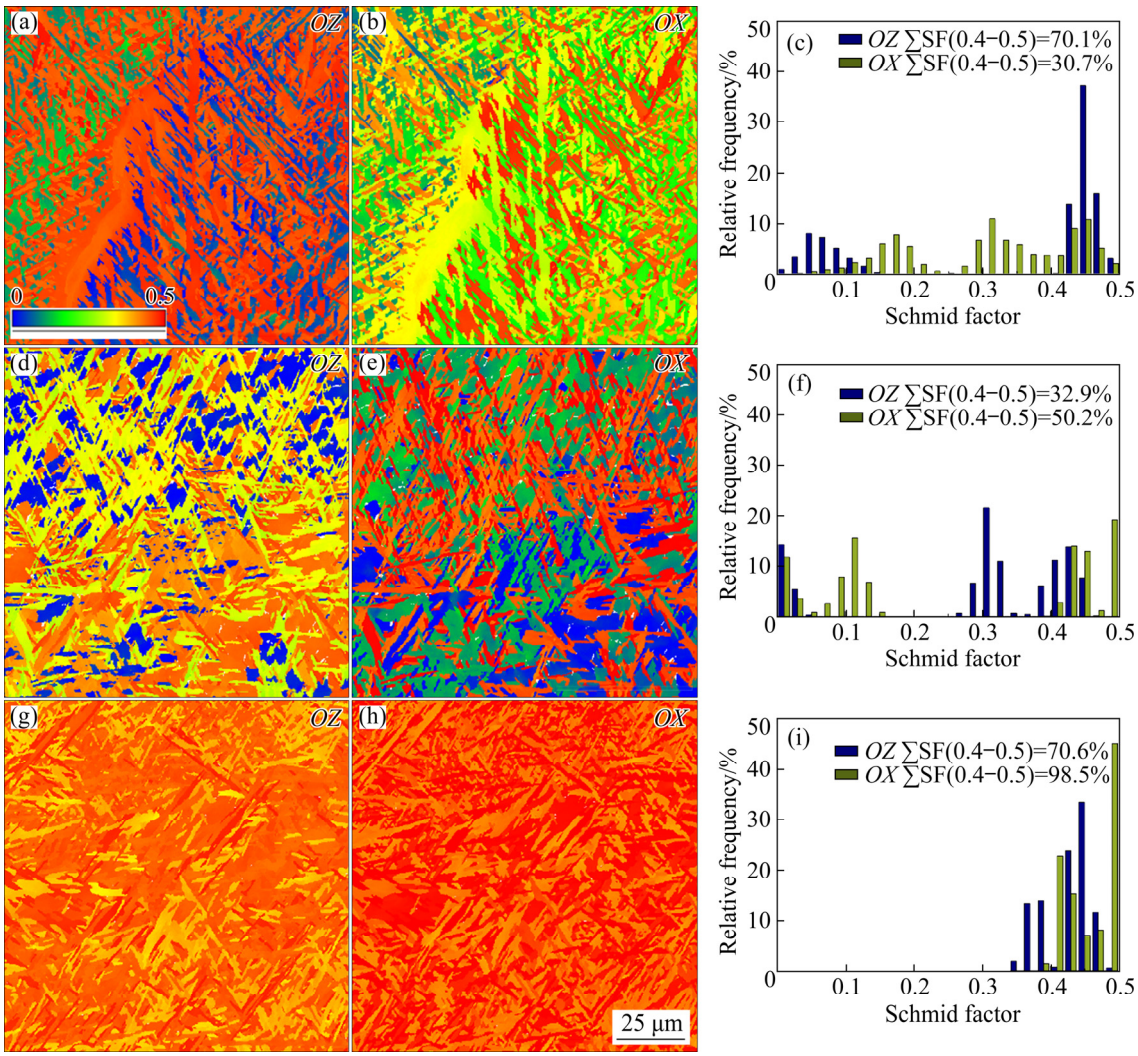

Fig. 6 Schmid factor (SF) maps and relative frequency of SF for as-built sample (a−c) and samples processed at 100 V (d−f) and 130 V (g−i) (Basal slip systems in the as-built condition and the sample processed at 100 V, and pyramidal slip systems in the sample processed at 130 V)

OX and *OZ* directions. This further confirms that the anistropy of YS in these two samples is related to *α* lath. Large SF means that slip system can be easily activated by applied stress [30]. When the as-built sample was deformed along *OZ* and *OX* directions, the basal slip exhibited ΣSF(0.4−0.5) of 70.1% and 30.7%, respectively. This is suggested to be mainly responsible for the larger YS when the sample was deformed along *OX* direction than that deformed along *OZ* direction. When the sample processed at 100 V was deformed along *OZ* and *OX* directions, the corresponding ΣSF(0.4−0.5) are 32.9% and 50.2%, respectively. This suggests that other factors should be considered to influence the anistropy in YS. From Fig. 3, the dislocation density of the sample processed at 100 V is quite larger than that of other two samples, indicating that the influence of dislocation on the activation of slip system cannot be ignored. Most of dislocation array are preferentially perpendicular to the long axis of grains, which implies that the distribution of dislocations may partially contribute to the anistropy in YS. In addition, the distributions of SF in the sample processed at 100 V are quite scattered. Mechanical interaction among the adjacent "soft" and "hard" grains may influence the anistropy in YS [31]. However, both the roles of the distribution of dislocations and SF in determining the mechanical anistropy require further investigation to reveal the detailed mechanism. In the sample processed at 130 V, the SFs mainly locate in the "soft" region, namely, the values of ΣSF(0.4−0.5) are 70.6% and 98.5% for the tensile deformations along *OZ* and *OX* directions, as shown in Fig. 6(i). Furthermore, for the deformation along *OZ* direction, the rest of SF values mainly distribute in the range of 0.35−0.4 (ΣSF(0.35−0.4)=29.4%). This means that the pyramidal slip system can be easily and equivalently activated when the samples were deformed along these directions. As a result, the near-isotropic YS was observed in the sample processed at 130 V.

It should be highlighted that in comparison with conventional heat treatment, electropulsing treatment is characterized by time-saving and localized heating features. This means that such a processing can be applied to efficiently tailoring the properties of the parts produced by AM to meet some specific requirements. In this aspect, further investigation is necessary to tailor the processing parameters of electropusling for the purpose of obtaining a comprehensive relationship of processing−microstructure−mechanical properties, especially the relationship between the processing and the texture evolution.

4 Conclusions

(1) Electropulsing does not change the morphology of columnar *β* grains. With increasing applied voltages from 0 to 130 V, the microstructure within *β* grains changes in the following sequence: *α′* martensite → colony *α* structure → basket-weave *α* structure. Electropulsing reduces the aspect ratio of *α* lath, which can be explained by thermal grooving and boundary splitting mechanism, and weakens the texture within *β* grains.

(2) The as-built sample is characterized by the anisotropy in YS. With increasing applied voltages, the anisotropy in YS decreases. The sample processed at 130 V shows the near-isotropic YS, which is attributed to the almost equivalent distribution of SF when deformed along different directions.

Acknowledgments

The authors are grateful for the financial supports from the National Key R&D Program of China (No. 2017YFE0123500).

References

[1] KOBRYN P A, SEMIATIN S L. The laser additive manufacture of Ti−6Al−4V [J]. JOM, 2001, 53: 40−42.

[2] LIU Shun-yu, SHIN Y C. Additive manufacturing of Ti6Al4V alloy: A review [J]. Materials & Design, 2019, 164: 107552.

[3] LI Neng, HUANG Shuai, ZHANG Guo-dong, QIN Ren-yao, LIU Wei, XIONG Hua-ping, SHI Gong-qi, BLACKBURN J. Progress in additive manufacturing on new materials: A review [J]. Journal of Materials Science & Technology, 2019, 35: 242−269.

[4] AZARNIYA A, COLERA X G, MIRZAALI M J, SOVIZI S, BARTOLOMEU F, St WEGLOWSKI M K, WITS W W, YAP C Y, AHN J, MIRANDA G, SILVA F S, MADAAH HOSSEINI H R, RAMAKRISHNA S, ZADPOOR A A. Additive manufacturing of Ti−6Al−4V parts through laser metal deposition (LMD): Process, microstructure, and mechanical properties [J]. Journal of Alloys and Compounds, 2019, 804: 163−191.

[5] GUO Kuai-kuai, LIU Chang-sheng, CHEN Sui-yuan, DONG Huan-huan, WANG Si-yu. High pressure EIGA preparation and 3D printing capability of Ti−6Al−4V powder [J].

Transactions of Nonferrous Metals Society of China, 2020, 30: 147−159.

[6] ZHU Yan-yan, CHEN Bo, TANG Hai-bo, CHENG Xu, WANG Hua-ming, LI Jia. Influence of heat treatments on microstructure and mechanical properties of laser additive manufacturing Ti−5Al−2Sn−2Zr−4Mo−4Cr titanium alloy [J]. Transactions of Nonferrous Metals Society of China, 2018, 28: 36−46.

[7] HAN Li-ying, WANG Cun-shan. Microstructure and properties of $Ti_{64.51}Fe_{26.40}Zr_{5.86}Sn_{2.93}Y_{0.30}$ biomedical alloy fabricated by laser additive manufacturing [J]. Transactions of Nonferrous Metals Society of China, 2020, 30: 3274−3286.

[8] WU Xin-hua, LIANG Jing, MEI Jun-fa, MITCHELL C, GOODWIN P S, VOICE W. Microstructures of laser-deposited Ti−6Al−4V [J]. Materials & Design, 2004, 25: 137−144.

[9] CARROLL B E, PALMER T A, BEESE A M. Anisotropic tensile behavior of Ti−6Al−4V components fabricated with directed energy deposition additive manufacturing [J]. Acta Materialia, 2015, 87: 309−320.

[10] ALCISTO J, ENRIQUEZ A, GARCIA H, HINKSON S, STEELMAN T, SILVERMAN E, VALDOVINO P, GIGERENZER H, FOYOS J, OGREN J, DOREY J, KARG K, MCDONALD T, ES-SAID O S. Tensile properties and microstructures of laser-formed Ti−6Al−4V [J]. Journal of Materials Engineering and Performance, 2011, 20: 203−212.

[11] TODARO C J, EASTON M A, QIU D, ZHANG D, BERMINGHAM M J, LUI E W, BRANDT M, STJOHN D H, QIAN M. Grain structure control during metal 3D printing by high-intensity ultrasound [J]. Nature Communications, 2020, 11: 142.

[12] CHOI G, CHOI W S, HAN J, CHOI P. Additive manufacturing of titanium-base alloys with equiaxed microstructures using powder blends [J]. Additive Manufacturing, 2020, 36: 101467.

[13] ZOU Zhi-yi, SIMONELLI M, KATRIB J, DIMITRAKIS G, HAGUE R. Refinement of the grain structure of additive manufactured titanium alloys via epitaxial recrystallization enabled by rapid heat treatment [J]. Scripta Materialia, 2020, 180: 66−70.

[14] ZHANG Du-yao, QIU Dong, GIBSON M A, ZHENG Yu-feng, FRASER H L, St JOHN D H, EASTON M A. Additive manufacturing of ultrafine-grained high-strength titanium alloys [J]. Nature, 2019, 576: 91−95.

[15] ZOU Zhi-yi, SIMONELLI M, KATRIB J, DIMITRAKIS G, HAGUE R. Microstructure and tensile properties of additive manufactured Ti−6Al−4V with refined prior-β grain structure obtained by rapid heat treatment [J]. Materials Science and Engineering A, 2021, 814: 141271.

[16] ZHAO Shi-teng, ZHANG Ruo-peng, CHONG Yan, LI Xiao-qing, ABU-ODEH A, ROTHCHILD E, CHRZAN D C, ASTA M, MORRIS J W, MINOR A M. Defect reconfiguration in a Ti−Al alloy via electroplasticity [J]. Nature Materials, 2021, 20: 468−472.

[17] WARYOBA D, ISLAM Z, REUTZEL T, HAQUE A. Electro-strengthening of the additively manufactured Ti−6Al−4V alloy [J]. Materials Science and Engineering A, 2020, 798: 140062.

[18] GAO J B, BEN D D, YANG H J, MENG L X, JI H B, LIAN D , CHEN J, YI J L, WANG L, LI P, ZHANG Z F. Effects of electropulsing on the microstructure and microhardness of a selective laser melted Ti6Al4V alloy [J]. Journal of Alloys and Compounds, 2021, 875: 160044.

[19] LI Ren-kai, WANG Hua-ming, HE Bei, LI Zhuo, ZHU Yan-yan, ZHENG Dong-dong, TIAN Xiang-jun, ZHANG Shu-quan. Effect of α texture on the anisotropy of yield strength in Ti−6Al−2Zr−1Mo−1V alloy fabricated by laser directed energy deposition technique [J]. Materials Science and Engineering A, 2021, 824: 141771.

[20] TSENG J, HUANG W, CHANG W, JEROMIN A, KELLER T F, SHEN J, CHUANG A C, WANG C C, LIN B H, AMALIA L, TSOU N T, SHIH S, HUANG E W. Deformations of Ti−6Al−4V additive-manufacturing-induced isotropic and anisotropic columnar structures: In situ measurements and underlying mechanisms [J]. Additive Manufacturing, 2020, 35: 101322.

[21] REN Y M, LIN X, FU X, TAN H, CHEN J, HUANG W D. Microstructure and deformation behavior of Ti−6Al−4V alloy by high-power laser solid forming [J]. Acta Materialia, 2017, 132: 82−95.

[22] BAYKASOGLU C, AKYILDIZ O, CANDEMIR D, YANG Q C, TO A C. Predicting microstructure evolution during directed energy deposition additive manufacturing of Ti−6Al−4V [J]. Journal of Manufacturing Science and Engineering, 2018, 140: 051003.

[23] GORUNOV A I. Additive manufacturing of Ti6Al4V parts using ultrasonic assisted direct energy deposition [J]. Journal of Manufacturing Processes, 2020, 59: 545−556.

[24] YANG Zhi-nan, JIANG Feng, WANG Xu-biao, QU Lin, LI Yan-guo, CHAI Lin-jiang, ZHANG Fu-cheng. Effect of electropulsing treatment on microstructure and mechanical properties of a deformed ZrTiAlV alloy [J]. Materials, 2019, 12: 3560.

[25] WARYOBA D, ISLAM Z, REUTZEL T, HAQUE A. Electro-strengthening of the additively manufactured Ti−6Al−4V alloy [J]. Materials Science and Engineering A, 2020, 798: 140062.

[26] ROY S, SUWAS S. Orientation dependent spheroidization response and macro-zone formation during sub β-transus processing of Ti−6Al−4V alloy [J]. Acta Materialia, 2017, 134: 283−301.

[27] ZUO Yu-ting, WANG Shu-ming, LI Cong, ZHANG Li-min, ZHU Yan-yan. Multi-scale texture analysis of titanium alloy made by laser additive manufacturing [J]. Rare Metal Materials and Engineering, 2021, 50: 1365−1370.

[28] DEBROY T, WEI H L, ZUBACK J S, MUKHERJEE T, ELMER J W, MILEWSKI J O, BEESE A M, WILSON-HEID A, DE A, ZHANG W. Additive manufacturing of metallic components – Process, structure and properties [J]. Progress in Materials Science, 2018, 92: 112−224.

[29] CEPEDA-JIMÉNEZ C M, POTENZA F, MAGALINI E, LUCHIN V, MOLINARI A, PÉREZ-PRADO M T. Effect of energy density on the microstructure and texture evolution of Ti−6Al−4V manufactured by laser powder bed fusion [J]. Materials Characterization, 2020, 163: 110238.

[30] LU S L, TANG H P, NAI S M L, SUN Y Y, WANG P, WEI J, QIAN M. Intensified texture in selective electron beam melted Ti−6Al−4V thin plates by hot isostatic pressing and its fundamental influence on tensile fracture and properties [J]. Materials Characterization, 2019, 152: 162−168.

[31] KAWANO Y, SATO M, MAYAMA T, MITSUHARA M, YAMASAKI S. Quantitative evaluation of slip activity in polycrystalline α-titanium considering non-local interactions between crystal grains [J]. International Journal of Plasticity, 2020, 127: 102638.

电脉冲处理对激光沉积 Ti−6Al−4V 合金强度各向异性的影响

王福斌[1]，刘宇珂[1]，佟运祥[1]，张 翀[1]，姜风春[2]，王建东[2]

1. 哈尔滨工程大学 材料科学与化学工程学院 材料加工及智能制造研究所，哈尔滨 150001；
2. 哈尔滨工程大学 材料科学与化学工程学院 超轻材料与表面技术教育部重点实验室，哈尔滨 150001

摘 要：为消除激光沉积 Ti−6Al−4V 合金的强度各向异性，利用拉伸试验、光学显微组织观察、扫描电子显微观察、电子背散射衍射分析和透射电子显微观察研究电脉冲对激光沉积 Ti−6Al−4V 合金显微组织与强度的影响。结果显示，随着施加电压从 0 增加到 130 V，β 柱状晶内的显微组织按如下顺序演化：α' 马氏体 → 集束 α 组织 → 网篮 α 组织。130 V 电脉冲处理会弱化 β 柱状晶内马氏体织构。沉积态 Ti−6Al−4V 合金表现出约 6.2%的屈服强度各向异性；经 130 V 的电脉冲处理后，屈服强度各向异性减小到 0.6%。这主要是由于沿不同方向变形时，130 V 电脉冲处理样品表现出近似相同的施密特因子分布。

关键词：激光沉积；Ti−6Al−4V 合金；屈服强度；各向异性；电脉冲

(Edited by Bing YANG)